Accessing the Solar System With a Small Solar Sail

Jeremy S. Neubauer
Graduate Research Assistant

Dr. Michael Swartwout
Faculty Advisor

Washington University in St. Louis, MO 63130

Solar sailing is a proposed means of space propulsion in which a reflective surface collects momentum from solar photons to accelerate a vehicle. The current trend within the solar sailing community is to increase sail size as solar sailing technologies advance, allowing for larger payloads and higher accelerations. However, with the miniaturization of modern payloads, sail sizes can be dramatically reduced while still providing useful propulsion. These smaller micro-sails offer several advantages over larger sails, such as reduced cost and complexity and increased reliability and maneuverability.

This paper examines the design of an Earth escape mission and micro-sail intended to improve access to the solar system and deep space, keeping a practical eye on cost, reliability, and feasibility of manufacture. The optimal sail configuration is evolved from this design study and simulated in Earth orbit; results show that a sail as small as 150 m^2 can escape from a GTO carrying a 3 kg payload. Several examples of enabled missions are discussed.

Introduction

Solar sailing is a proposed means of space propulsion in which a large reflective surface collects momentum from solar photons to accelerate a vehicle. The most obvious benefit of solar sailing is its near-infinite energy source, providing a small, continuous thrust to enable faster and cheaper high-orbit-energy missions.

The concept of solar sailing was originally conceived in the 1920s, though with the state of available technology it was purely science fiction. It again received attention in the 1970s per NASA's Halley Comet Rendezvous mission, in the 1980s by U3P's proposed moon race, and in the 1990s by a proposed Mars race[1]. Yet none of these efforts have resulted in a single solar sail flight, due largely to the same ailment present at solar sailing's conception: insufficient technology. Since the propulsive force generated by a reflected photon is extremely small, solar sails with large reflective-area-to-mass ratios are necessary to produce measurable accelerations. These craft must first expand from stowed volumes smaller than a few cubic meters to deployed sails the size of a city block and larger, then be robust enough to endure the space environment for years. This task mandates the use of advanced materials and gossamer structures that are only now beginning to mature.

Today, the miniaturization of modern technology has reduced payload masses and recent advances in deployable structures technology have reduced the mass of a sail's support structure, finally making solar sailing a feasible and competitive mission implementation alternative. Accordingly, several different solar sailing projects are currently in the works: the Planetary Society's *Cosmos 1*[2], Team Encounter's *Encounter*[3], and DLR's *ODISSEE*[4].

Traditionally, solar sails have been envisioned as massive crafts, and this is reflected in the aforementioned sail projects. In fact, the current trend

is to increase sail size as technology advances, illustrated in Fig. 1. However, the miniaturization of payloads is beginning to negate the need for such large sails. For payloads of a few kilograms, sails of only a few hundred square meters can supply useable propulsion. These small micro-sails[i] offer superior maneuverability compared to their larger siblings, suiting them to dynamically demanding missions like Earth orbit and escape where large sails would likely fail. In fact, maneuverability increases sufficiently to enable micro-sails to escape from highly eccentric Geosynchronous Transfer Orbits (GTOs)—favored for the high frequency and lower cost secondary payload opportunities on GTO launch vehicles.

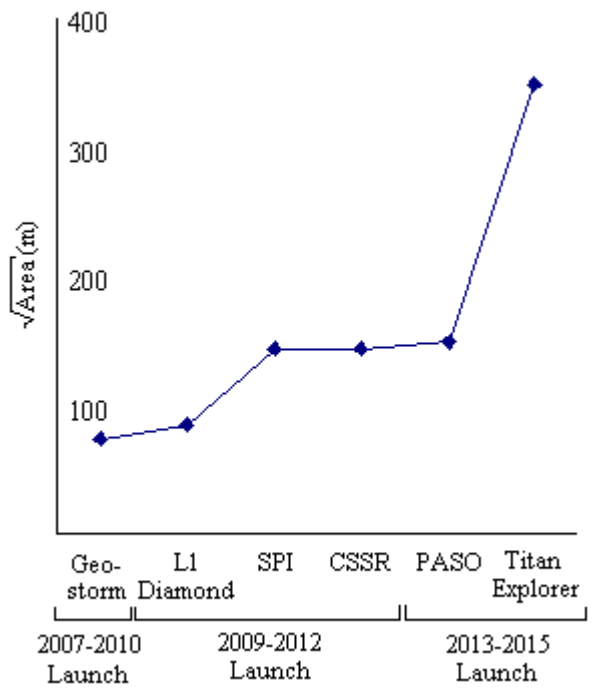

Fig 1 Trend to Increase Sail Size as Technology Advances[5]

Small sails offer further benefits concerning stowage, deployment, and cost. The smaller deployed dimensions allow both a smaller stowed volume and a simpler packing scheme. In turn, this simpler packing scheme can lead to more efficient and reliable deployment methods. Consequently, the complete design of a micro-sail is much less complex than that of a large sail, reducing cost while increasing the probability of mission success. Combining their benefits of reduced cost and smaller stowed volume, micro-sails could enable "swarm" missions, where dozens or even hundreds of stowed sails are launched on a single vehicle and flown together in place of a single large sail. This further increases the probability of mission success, as a failure of one sail would not terminate the entire mission.

This paper examines the design of an Earth escape mission and micro-sail intended to improve access to the solar system and deep space, making design choices that will maximize feasibility and reliability, and possibly minimize cost. Once the mission plan is evolved, a scalability and configuration analysis will be completed to select the optimal sail design for said plan. This sail will be simulated in the Earth orbit stages of the mission, its performance assessed, and a few enabled missions discussed.

Solar Sailing Physics

Quantum physics' wave-particle duality view of the photon teaches that photons have momentum. Therefore, when light impacts an object, it transfers some of this momentum to that object, generating a force. Considering the optical properties of the impacted object, there exist four force components: absorption, specular reflection, diffuse reflection, and emission, illustrated in Fig. 2 and defined in Eqs. (1-4). Notation for the figure and equations is defined in Table 1.

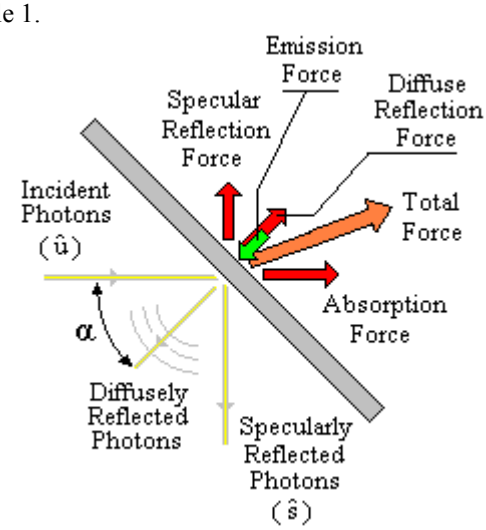

Fig. 2 Optical Model Solar Force Components

[i] Micro-sails are defined as solar sails with total reflective areas ranging from 100 to 1000 m^2.

$$F_{absorption} = PA_i\hat{u} \quad (1)$$

$$F_{specular_reflection} = -(ls)PA_i\hat{s} \quad (2)$$

$$F_{diffuse_reflection} = (1-s)lB_f PA_i\hat{n} \quad (3)$$

$$F_{emission} = \frac{\sigma T^4}{c}\left(\varepsilon_f B_f - \varepsilon_b B_b\right)\hat{n} \quad (4)$$

Table 1 Optical Model Solar Force Notation

Vectors	
$\hat{n}$	Sail Normal Vector
$\hat{u}$	Sunline Vector
$\hat{s}$	Specular Reflection Vector
Optical Properties	
B_f	Non-Lambertian coefficient (front side)
B_b	Non-Lambertian coefficient (back side)
ε_f	Emissivity (front side)
ε_b	Emissivity (back side)
l	Reflectivity
s	Specular Reflectivity
Other Notation	
A_i	Incident Area, $A_i = A(\hat{u}\bullet\hat{n})$
P	Solar Pressure, $P = 4.563\cdot 10^{-6}\, N\cdot m^{-2}$
T	Sail Temperature
σ	Boltzmann's Constant
c	Speed of Light

The emissive force can be converted to a function of sail orientation using the steady-state temperature of the sail, yielding Eq. (5). The resultant total force (Eq. (6)) is a nonlinear function of the solar incidence angle, α, varying in both magnitude and direction.

$$F_{emission} = (1-s)\left(\frac{\varepsilon_f B_f - \varepsilon_b B_b}{\varepsilon_f + \varepsilon_b}\right)PA(\hat{u}\bullet\hat{n})n \quad (5)$$

$$\vec{F} = PA(1-ls)(\hat{u}\bullet\hat{n})\hat{u} + PA\left[2ls(\hat{u}\bullet\hat{n})^2 + (1-s)\left(lB_f + \frac{\varepsilon_f B_f - \varepsilon_b B_b}{\varepsilon_f + \varepsilon_b}\right)(\hat{u}\bullet\hat{n})\right]\hat{n} \quad (6)$$

A common metric in assessing the performance of a solar sail is its characteristic acceleration—the maximum acceleration a sail can generate 1 AU from the sun. Consolidating the optical properties of the sail into an effective efficiency, η, the characteristic acceleration, a_0, of a sail is given by Eq. 7:

$$a_0 = 2\eta PA/m \quad (7)$$

Due to the extremely small solar pressure, a_0 is on the order of 1 mm/s^2. Though this may seem trivial, the thrust is continuous and the energy source practically limitless. As will be seen, sails with an a_0 as small as 0.27 mm/s^2 can escape from Earth orbit.

Earth Escape Mission Plan

Table 2 Micro-Sail Earth Escape Mission Plan

	Stage	Duration
1	Launch into GTO	~1 hr.
2	Cruise to Apogee	~ 6 hr.
3	Boost Perigee	~1 min
4	Hibernation	0 to 365 days
5	Deployment	30 min.
6	Earth Escape	160 to 381 days
	Total Escape Time:	**160.3 to 746.3 days**

The total mission plan and escape time is shown above in Table 2. The mission begins in a secondary payload position deployed in GTO. This launch was selected for its high availability, low cost, and the opportunity to send multiple sailcraft on a single launch, making the solar system accessible to as many explorers and entrepreneurs as possible.

Once in orbit, the stowed craft will be required to boost its perigee above the effects of the atmosphere, to a level where solar forces can overcome drag forces. The amount of boost will vary with the particular time and orientation of the initial orbit, as the atmosphere varies vastly with time, latitude and longitude, and altitude. It is generally assumed that atmospheric effects are negligible above altitudes of 1000 km, so, as a worst-case scenario, it will be required to boost the perigee altitude to this level[6].

The question may arise, if a thruster is incorporated to boost the perigee, why not use the thruster to boost the craft out of Earth orbit? As shown in Table 3, the

answer lies with the size of the thruster. Assuming a perigee altitude of 500 km, the ΔV required to raise the perigee to 1000 km is two orders of magnitude less than that required to elevate the orbit to a Geosynchronous Earth Orbit (GEO) or escape. Thus, a simple and inexpensive cold-gas thruster could be employed, then jettisoned after the maneuver.

Table 3 ΔV Requirements for Altering a GTO

Orbit Change	ΔV
500 km to 1000 km perigee	49.6 m/s
GTO to GEO	1450 m/s
GTO to Escape	4350 m/s

In orbit, a locally-optimal steer law will direct the sail's orientation. This steer law maximizes the instantaneous change in orbital energy by maximizing the dot product of the solar force and the sail's velocity vector[7]. Fig. 3 illustrates the force direction of this steer law with red arrows along the orbit trajectory. Note that the only available method to control force direction is to control sail orientation, hence it becomes essential that the sail's rotational dynamics be decoupled from its translational dynamics via sufficient control authority, such that energy is added to the orbit as efficiently as possible. If the sail's attitude control system is not powerful enough to accurately track the steer law, escape from Earth orbit can be delayed indefinitely.

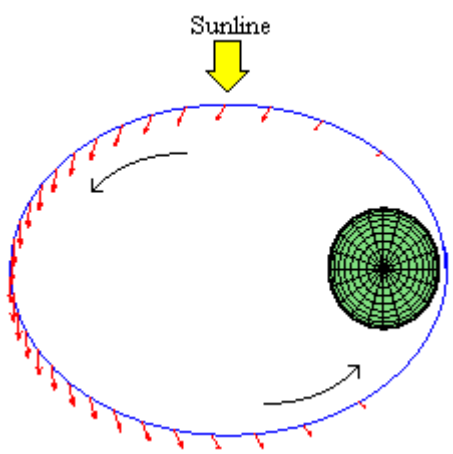

Fig. 3 Locally-Optimal Steer Law Force Direction

Two more conditions must be met for a solar sail to escape Earth orbit using this steer law: the sail must exhibit a characteristic acceleration of 0.270 mm/s^2 or greater[8], and sail deployment must coincide with the craft's optimal initial orbit orientation. Most initial orbit orientations result in a trajectory with a rapidly increasing eccentricity, ultimately leading to the sail crashing. Optimal initial orbit orientations, shown in Fig. 4, first elevate the orbit perigee, leading to the safest and most efficient escape. Coincidentally, these orbit orientations are also the optimal orientations for avoiding atmospheric effects, as the sail presents its smallest frontal area at perigee.

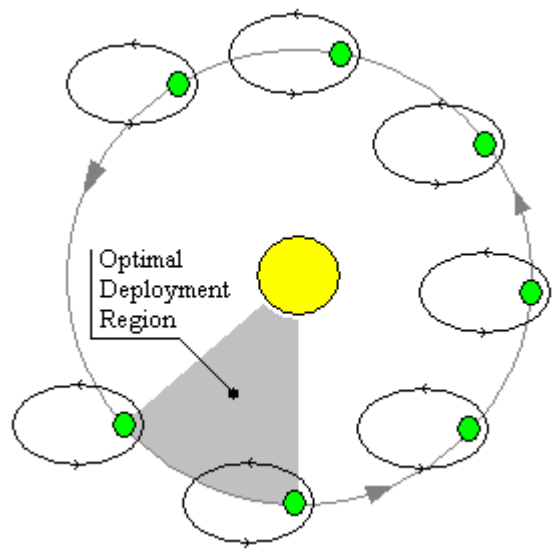

Fig. 4 Optimal Initial Orbit Orientation for Solar Sail Deployment[ii]

Sail Configuration

Reducing the size of a solar sail offers several benefits. First, with a smaller sail comes a much smaller moment of inertia, making quicker rotations possible with a less powerful control system. Second, smaller deployed dimensions correspond to smaller stowed dimensions, making it easier to comply with the volume constraints of the secondary payload slots on GTO launch vehicles. Finally, shorter booms and smaller sail panels are more feasible and less expensive to manufacture. These reasons make it desirable to implement a micro-sail.
Due to the smaller scale of a micro-sail, as well as the demanding mission plan, the 'standardized' four boom sail may not be the optimum sail configuration.

[ii] Note that the optimal deployment region is a function of the position and angle of the GTO orbit relative to the sun, not merely of the Earth's season.

Therefore, other central payload, *n*-spar sail configurations will be investigated. These sails consist of a central payload from which *n* booms (spars) extend straight outward. A 3-spar sail looks like a triangle, a 4-spar sail looks like a square, etc., as seen in Fig. 5.

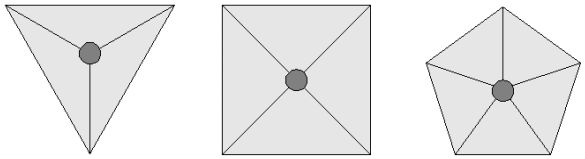

Fig. 5 3-, 4-, and 5- Spar Sail Configurations

Disregarding power- and fuel-based control methods such as reaction wheels and thrusters, two options exist for control of this sail: center of mass (CM) control, via mounting the payload on a gimbaled boom, and center of pressure control, via vanes on the tips of the spars. When implementing CM control, moving the payload creates a center of mass / center of pressure offset, resulting in a torque on the craft. With vane control, small reflective surfaces are oriented to redirect a fraction of the total solar force, generating a torque.

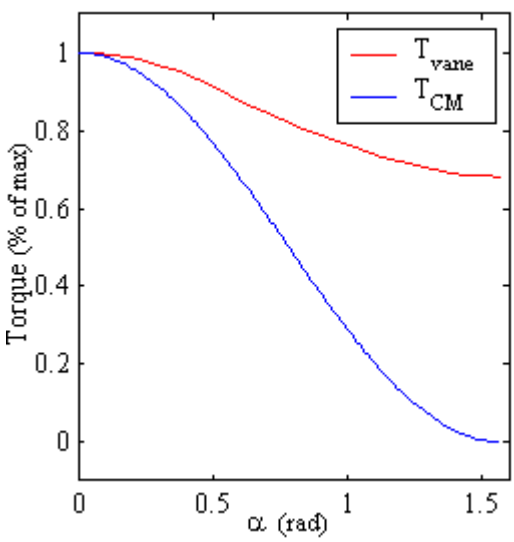

Fig. 6 Control Torque vs. Solar Incidence Angle (α) for Vane and CM Control

CM control offers the largest maximum control torque for yaw and pitch; however, it is highly nonlinear, and an auxiliary control system is necessary to provide roll torques. Vane control offers a lower maximum torque, but is more consistent as the solar incidence angle changes (Fig. 6) and can control rotations in all three axes. Due to the reduced inertia of the craft's small scale, vanes alone are sufficient for control—avoiding the added complexity, mass, and nonlinearity of CM control.

Scaling the n-Spar Sail

To select the size, *A*, and number of spars, *n*, a scalability analysis is in order. First, a constant payload mass, m_p, of 3 kg is assumed, and a mass allocation of 65 g for the actuation of each vane will be made, m_v.

Second, the sail film must be designed. Several factors must be considered, including the optical properties of the film, the areal density of the film, and the durability of the film—such that it will survive the rigors of both flight in space and handling on the ground. A promising candidate is SRS Technologies' CP1, a Kapton-based polymer with embedded carbon fibers acting as rip-stops. Currently, CP1 is available in thicknesses down to 2.5 µm, coated with a 0.1 µm layer of aluminum, while smaller thicknesses are in development[9]. For this study, a sail film comprised of a 1 µm CP1 substrate and a 0.1 µm aluminum coating will be assumed, resulting in a sail film density, ρ_s, of 1.70 g/m^2, illustrated in Fig. 7. The duty of the sail film is such that it does not need to scale with the size of an *n*-spar sail, and therefore the film density will remain constant over all *n* and *A*.

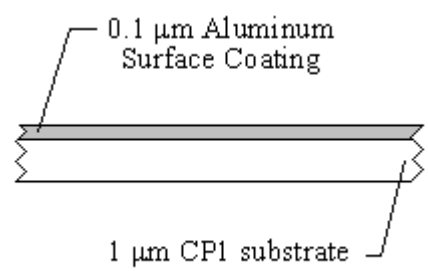

Fig. 7 Sail Film Cross-Section

Third, the boom design must be chosen. Many options arise: pressure-rigidized aluminum-polymer laminates, Second Order Transition Change (SOTC) composites,

thermally cured thermoset composites, etc.[10]. Of particular interest are the Carbon Fiber Reinforced Plastic (CFRP) booms designed by the German Aerospace Center (DLR)[4]. As shown in Fig. 8, the near circular cross section of the booms can be pressed flat, then coiled and stowed into a small volume. The strain energy stored in the boom while stowed is sufficient to deploy the boom and restore the original cross section. This boom also offers high stiffness, low density, and low thermal distortion. Due largely to the simplicity and reliability of its deployment and rigidization method over that of other boom designs, DLR's deployable CFRP boom is the design of choice.

Fig. 8 DLR's Deployable CFRP Boom[4]

Scaling the boom design can be done in several ways, such as first calculating the maximum expected loads, then scaling the cross section to yield a proportional deflection or constant factor of safety against buckling. However, with the small size of micro-sails, these methods result in unreasonably small booms with diameters of only a few millimeters. Therefore, for this study it will be assumed that boom size is mandated by what is manufacturable, and, thusly, linear boom density will be constant across all n and A. Since the booms developed by DLR for a 1600 m^2 square sail have a linear density of 101 g/m, it will be assumed that the outer diameter can safely be reduced to yield a linear density, ρ_b, of 35 g/m for use in the much smaller micro-sails.

To begin scaling the sail, boom length is calculated as a function of n and A. Fig. 9 shows a single triangular section of an n-spar sail, from which the boom length may be evaluated (Eq. (8)).

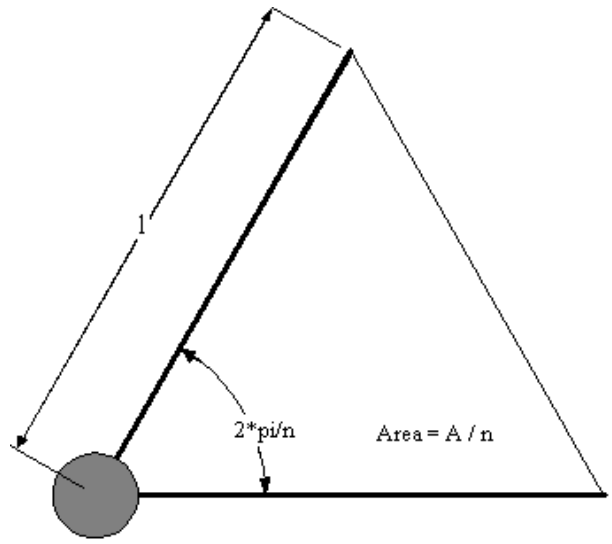

Fig. 9 A Single Section of an n-Spar Sail

$$l = \sqrt{\frac{A}{n\cos(\pi/n)\sin(\pi/n)}} \tag{8}$$

The total mass of the craft is now given by Eq. (9), and the characteristic acceleration is given by Eq. (10), where a_v is the ratio of total vane area to sail area.

$$m = m_p + n * m_v + \rho_s A(1 + a_v) + n * l * \rho_b \tag{9}$$

$$a_o = 2\eta PA(1 + a_v)/m \tag{10}$$

Two metrics will be used to assess control scaling: the maximum angular acceleration of the craft, and the ratio of control torque to gravity gradient torque at the orbit perigee. First, the polar moment of inertia of the micro-sail is computed, using Eq. (11),

$$J_p = n\left(J_T + \frac{\rho_b l^3}{6} + m_v l^2\right) + \rho_s a_v A l^2 \tag{11}$$

where J_T is the inertia of a triangular section of sail film, given by Eq. (12).

$$J_T = \rho_s \left(\frac{A}{n}\right)^2 \left(\frac{1}{2}\cot(\pi/n) + \frac{1}{6}\tan(\pi/n)\right) \tag{12}$$

Since the other two principal moments of inertia (those of yaw and pitch) are equivalent, the difference

between the maximum and minimum moment of inertia and the inertia for yaw/pitch is given by Eq. (13).

$$J_{yaw/pitch} = \left(J_{\max} - J_{\min}\right) = \frac{1}{2} J_p \tag{13}$$

The control torque of the sail must be calculated for both the yaw and pitch axis—unlike the moments of inertia, torques for yaw and pitch are dissimilar. These torques are given by Eqs. (14) and (15).

$$T_{pitch} = \left(2\eta P a_v A^{3/2}\right)\left(\frac{\sum_{i=1}^{floor(n/2)} \sin\left(\beta + (i-1)\frac{2\pi}{n}\right)}{n\sqrt{n\cos(\pi/n)\sin(\pi/n)}}\right) \tag{14}$$

$$T_{yaw} = \left(2\eta P a_v A^{3/2}\right)\left(\frac{\sum_{i=1}^{floor(n/2)} \sin\left(i\frac{2\pi}{n}\right)}{n\sqrt{n\cos(\pi/n)\sin(\pi/n)}}\right) \tag{15}$$

$$\beta = \frac{\pi}{2} - \frac{\pi}{n} floor\left(\frac{n}{2} - 1\right) \tag{16}$$

Eqs. (14-16) reveal two separate trends in yaw and pitch torques for sails of even and odd n. As illustrated in Fig. 10, sails with odd n have a consistently closer yaw and pitch torque than those of even-n sails, giving odd-n sails superior multi-axis maneuverability.

The first control metric, maximum angular acceleration, can now be attained by dividing the control torque by the moment of inertia. To include the disparity between the yaw and pitch control torques, Eq. (17) uses the average of those torques.

$$\ddot{\gamma}_{\max} = \frac{T_{pitch} + T_{yaw}}{2J_{yaw/pitch}} \tag{17}$$

The maximum gravity gradient torque is given by Eq. (18), where μ_e is the Earth's gravitational constant, and R is the distance from the center of the Earth to the craft at perigee.

$$T_{gg} = \frac{3\mu_e}{2R^3}\left(J_{\max} - J_{\min}\right) \tag{18}$$

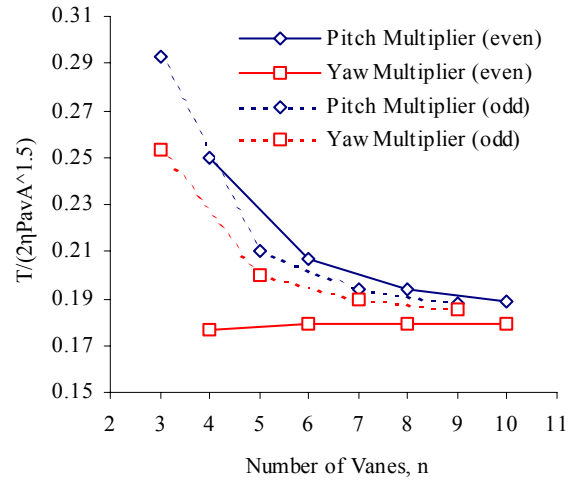

Fig. 10 Control Torque as a Function of n

The second control metric is attained by dividing the pitch torque by the gravity gradient torque, creating Eq. (19).

$$\frac{T_{pitch}}{T_{gg}} = \frac{4\eta P a_v A^{3/2} R^3}{3\mu_e\left(J_{\max} - J_{\min}\right)} \frac{\sum_{i=1}^{floor(n/2)} \sin\left(\beta + (i-1)\frac{2\pi}{n}\right)}{n\sqrt{n\cos(\pi/n)\sin(\pi/n)}} \tag{19}$$

The three main metrics—characteristic acceleration, maximum angular acceleration, and the ratio of maximum control torque to gravity gradient torque—are plotted in Fig. 11 for a sail with an a_v of 0.02. The plots of characteristic acceleration and rotational acceleration clearly show that a 3-spar sail is the optimal configuration. An argument could be made for the 4-spar sail, since it provides a larger ratio of control to gravity gradient torque; however, referring back to Fig. 10, the 3-spar sail has a much smaller disparity between yaw and pitch torques. The 3-spar sail also offers the added benefit of fewer parts—leading to lower overall mass and cost, and larger boom separation during deployment.

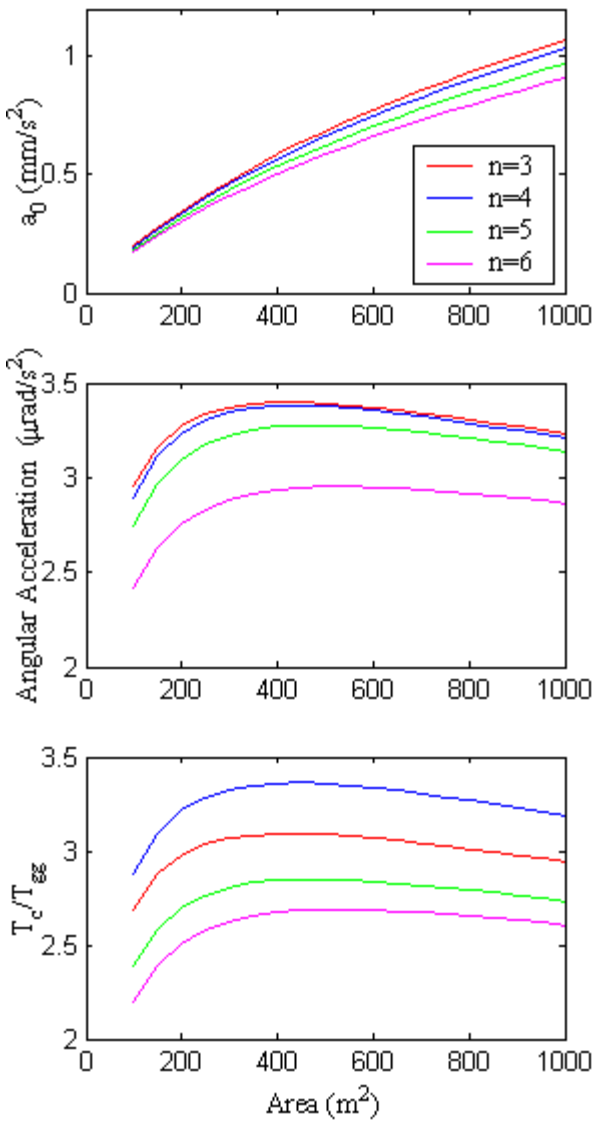

Fig. 11 Sail Design Metrics as a Function of n and A

Note that Fig. 11 shows only a slight linear decrease in rotational performance as A increases beyond 450 m^2. The subtlety of this slope may seem to negate the drive for building a micro-sail; however, the constant linear boom density assumption plays a large role. Scaling the boom size with A creates a much more dramatic exponential decrease in rotational performance with increasing A, which drives this study to focus on small sails.

For the 3-spar sail, maximum rotational performance occurs at an area of 450 m^2, providing a characteristic acceleration of 0.636 mm/s^2. Since this characteristic acceleration is more than ample to escape, area could be reduced to as low as 150 m^2. Though this decreases the characteristic acceleration to 0.274 mm/s^2, the stiffness of the craft and ease of manufacture would increase, while cost would decrease. The performance metrics and mass breakdown of both the 150 m^2 and 450 m^2 sails are compared below in Table 4.

Table 4 Micro-Sail Performance Metrics

Metric	**Value**	
	150 m^2 Sail	*450 m^2 Sail*
Mass	4.583 kg	5.929 kg
Payload	*3.000 kg*	*3.000 kg*
Control	*0.200 kg*	*0.210 kg*
Booms	*1.128 kg*	*1.954 kg*
Sail Film	*0.255 kg*	*0.765 kg*
Characteristic Acceleration	0.274 mm/s^2	0.636 mm/s^2
Max Angular Acceleration	3.156 μrad/s^2	3.397 μrad/s^2
T_c / T_{gg}	2.873	3.092

Orbit Simulation

To assist in selecting the optimal design, both the 150 m^2 and 450 m^2 3-spar sails will be evaluated in-flight. The orbit simulation will begin from a representative GTO, with the perigee boosted to 1000 km altitude to avoid atmospheric effects and sail deployment timed to coincide with the optimal orbit orientation.

When simulating the sail in Earth orbit, atmospheric, shadowing, and lunar gravitation effects are neglected, and sail rotation is constrained to one axis by aligning the GTO plane parallel to the ecliptic. Gravitation of the sun and Earth are included, and an optical solar force model is employed. The translational equations of motion are based in a sun-centered inertial coordinate frame, as seen in vector form in Eq. (19), where $\vec{F}$ is the solar induced force.

$$m\vec{a} = -\frac{\mu_s}{\vec{R}^3}\vec{R} - \frac{\mu_e}{\left(\vec{R}-\vec{R}_e\right)^3}\left(\vec{R}-\vec{R}_e\right) + \vec{F} \tag{20}$$

The rotational equation of motion is derived by summing the moments created by each vane with the gravity gradient torque, as shown in Eq. (20). $\vec{F}_i$ is the force generated by the ith vane, and $\vec{r}_i$ is the moment arm of that vane.

$$J\ddot{\gamma} = \sum_{i=1}^{3}\left(\vec{r}_i \times \vec{F}_i\right) + T_{gg} \tag{21}$$

A feedback linearization technique is implemented to linearize this function, then a PD controller is applied, optimized to minimize step response settling time. The orbit simulation is then run in Simulink, using an ode45 solver with relative and absolute tolerances of 1e-3 and a maximum step size of 120 seconds.

The optimized step responses for both the 150 and 450 m^2 are shown in Fig. 12, and the initial steer law tracking is shown in Fig. 13. Both plots reveal that the rotational performance of the two sails is nearly identical.

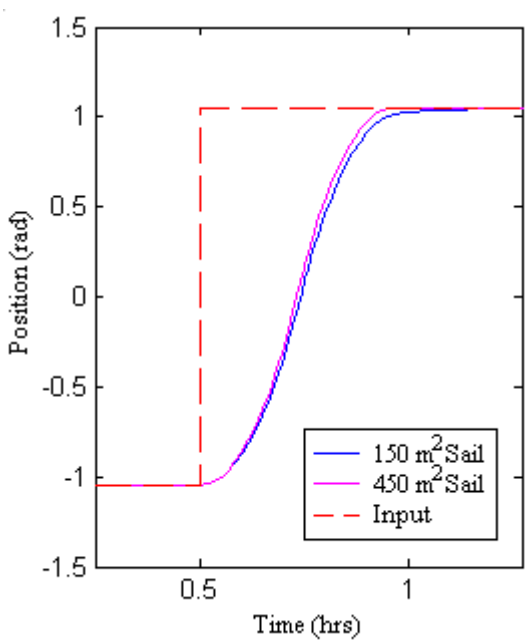

Fig. 12 Step Responses for 150 m^2 and 450 m^2 Micro-Sails

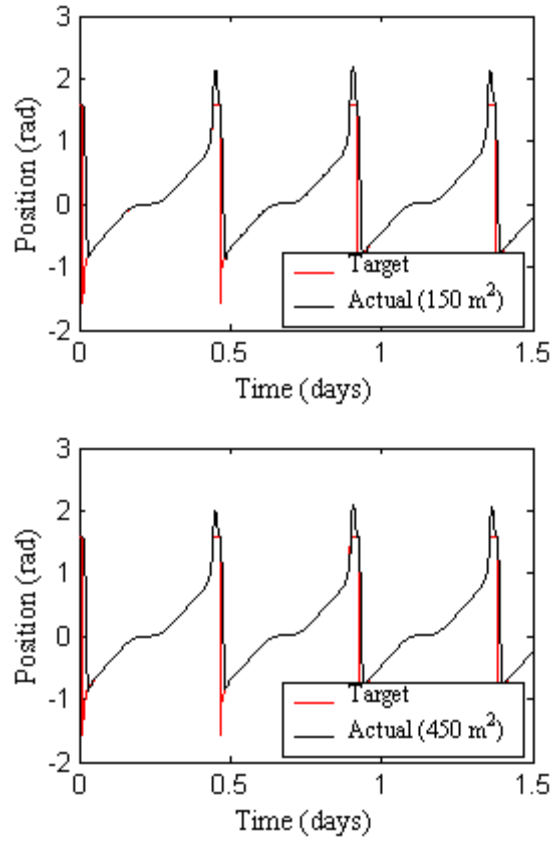

Fig. 13 Steer Law Tracking in a GTO for 150 m^2 and 450 m^2 Micro-Sails

Note the overshoot present in the steer law tracking at $\pi/2$. This is a combined effect of low available control torque, due to the sail being feathered to the sun, and high gravity gradient torque, due to the low perigee altitude. For larger sails, the gravity gradient torque overwhelms the attitude control system due to the crafts' large moments of inertia, increasing the magnitude of the overshoot and the resultant recovery time. This divergence from the steer law delays or impedes escape.

The small tracking errors of the simulated micro-sails, however, have a minimal impact on their overall orbit trajectories, as both sails escape. The 450 m^2 sail escapes Earth orbit in 159.7 days, much sooner than the 150 m^2 sail's 381.3 day escape time, due to the larger sail's higher characteristic acceleration.

Sail Sizing

The above analysis has shown that 150 to 450 m^2 3-spar micro-sails are capable of escaping a GTO with a 3 kg payload[iii]. Increasing the sail size within this range raises the characteristic acceleration and hastens escape, while decreasing size offers reduced cost, increased ease of manufacture, and increased stiffness and safety factors in the sail structure. As discussed above, rotational performance stays nearly constant.

Thus the final selection of sail size is a tradeoff between speed, cost, and reliability. As the importance of these three factors vary with the ultimate mission application and customer, sail sizing should be done on a case-by-case basis.

Example Missions

Micro-sails could enable many different missions. First and foremost, micro-sailing in Earth orbit offers a time- and cost-effective method for testing solar sailing technologies. Prototype construction is aided by the smaller dimensions and reduced cost, and with the ability to fly multiple crafts on a single GTO launch vehicle, multiple tests can be run quickly and inexpensively.

In the near term, small fleets of micro-sails could be deployed to make distributed, real time measurements of the magnetosphere. The required sensors and data handling equipment of this mission allow for payloads well under the examined size of 3 kg's, and with the secondary payload capacity of an Ariane 5 rocket of 960 kg[11], more than 200 of the 150 m^2 sails could be launched simultaneously.

As payloads are further miniaturized, micro-sails could investigate near Earth objects (NEOs), distant asteroids, and comets. In fact, this could become a common mission for said sails, as multiple cameras may already be onboard for position and attitude determination[12]. The increased maneuverability of the micro-sails could allow it to track and orbit their targets for extended periods of time, providing considerably more information than that gathered from the mere fly-by of larger, less agile sailcraft. Via formation flying of large numbers of micro-sails, small NEOs could be captured and delivered to the International Space Station, accomplishing similar goals as that of the proposed AsterAnts mission[13].

In the more distant future, as communication technology advances, micro-sails could even act as routers in an interplanetary IP infrastructure. This proposed wireless interplanetary internet creates a "network of internets", connecting planets and spacecraft to increase communication capabilities and assist exploration of the solar system[14]. With their long lifetime, ability to continually adjust their orbits and positions, and friendliness to large quantities, micro-sails could be an enabling technology for such a project.

Table 5 Example Micro-Sail Missions

Mission	Timeline	Necessary Technology Advancements
Distributed Measurement	Near-Term	Gossamer Structures
NEO Investigator	Mid-Term	Gossamer Structures, Imaging
NEO Capture & Return	Far-Term	Gossamer Structures, Imaging, Formation Flying
Interplanetary IP	Far-Term	Gossamer Structures, Communications

Conclusions

This study has shown how small micro-sails are capable of delivering payloads of a few kilograms beyond Earth orbit, due largely to the micro-sails' improved maneuverability. The optimal sail configuration was proven to be a 3-spar, central payload, vane control sail, incorporating technologies of the present and near future.

There are several advantages of these micro-sails. First, the small, and accordingly inexpensive nature of the craft allows small organizations and fledgling space programs previously constrained to Earth orbit access to the solar system. It also enables larger organizations to increase mission redundancy by sending multiple crafts in place of one. Furthermore, the unlimited energy source of solar sails can dramatically increase

[iii] Increasing the sail size above 450 m^2 will decrease the rotational performance, and soon require a rescaling of the boom size; decreasing the sail size below 150 m^2 will result in insufficient characteristic accelerations for the assumed payload.

mission life, and the continuous thrust can create non-Keplerian flight paths, making interesting new missions possible.

The dominant disadvantage of micro-sails are their necessarily long mission durations. This places high demands on all of the components of the sail and payload, as they must be durable enough to survive years of service in space. Long mission durations can also counter the discussed cost advantages of micro-sails with a rise in total operational costs. Another downside to these sails is their large size—although they are much smaller than most sail designs, they are still significantly larger than traditional spacecraft.

References

[1] McInnes, C.R., *Solar Sailing: Technology, Dynamics, and Mission Applications*, Springer Praxis Publishing, 1999.

[2] The Planetary Society, http://www.planetary.org/solarsail/index2.html

[3] Rogan, James, "Encounter 2001: Sailing to the Stars," *Proceedings of the 15th Annual AIAA/USU Conference on Small Satellites*, Logan, UT, August 2001.

[4] Leipold, M., et al., *Solar Sail Technology Development and Demonstration*, DLR, ESA/ESTEC, INVENT, JPL, 2000.

[5] Garbe, Gregory P., "Solar Sail Flight System Technology," presented at the Technology Planning Workshop for Space Technology 9 (ST9), Washington D.C., February 2003.

[6] Fieseler, P., "A Method for Solar Sailing in a Low Earth Orbit," *Acta Astronautica*, Vol. 43 (No. 9-10), Elsevier Science Ltd., 1998, p. 531-541.

[7] Coverstone-Carroll, Victoria, and John E. Prussing, "A Technique for Earth Escape Using a Solar Sail," *Advances in the Astronautical Sciences*, Vol. 103, Part I, Univelt, Inc., 1999, pp. 507-521.

[8] Ressler, Kyle T., "Design Analysis for Solar Sailing from Geosynchronous Transfer Orbit," *Proceedings of the 16th Annual AIAA/USU Conference on Small Satellites*, Logan, UT, August 2002.

[9] SRS Technologies, http://www.srs.com, 2003.

[10] Cadogan, David P., and S.E. Scarborough, "Rigidizable Materials for use in Gossamer Space Inflatable Structures," *Proceedings of the 42nd AIAA/ASME/ASCE/AHS/ASC Structures, Structural Dynamics, and Materials Conference & Exhibit*, Seattle, WA, April 2001.

[11] *Arianespace,* www.arianespace.com, 2003.

[12] Meller, David, Prapat Sripruetkiat, and Kristin Makovec, "Digital CMOS Cameras for Attitude Determination," *Proceedings of the 14th Annual AIAA/USU Conference on Small Satellites*, Logan, UT, August 2000.

[13] Globus, Al, Bryan Biegel, and Steve Traugott, *AsterAnts: A Concept for Large-Scale Meteoroid Return and Processing using the International Space Station*, NASA Ames Research Center, NAS Technical Report NAS-99-006.

[14] Burleigh, S., et al., "The Interplanetary Internet: A Communications Infrastructure for Mars Exploration," *Proceedings of the 53rd International Astronautical Congress*, Houston, TX, October 2002.